ULTRASONIC IMAGING 9, 203-219 (1987)

A TAYLOR SERIES EXPANSION FOR TIME SAVINGS IN ACCURATE COMPUTATION OF FOCUSED ULTRASOUND PRESSURE FIELDS

Timothy J. Hall, Ernest L. Madsen and James A. Zagzebski

Department of Medical Physics
University of Wisconsin
Madison, WI 53706

A model for the continuous wave (cw) pressure beam distribution of a focused axially symmetric ultrasonic radiator with constant radius of curvature involves integration of e^{ikr}/r over the surface of the radiator. (k is the complex wave number and r is the distance from a radiating area element to the field point.) A single integral form exists, and it is this form that is expanded in a Taylor series in frequency. Thus, when representing a pulse as a superposition of cw beams, the need to do numerical integrations for each one of a large number of frequencies is eliminated. Accuracy of the truncated Taylor series depends on the coordinates of the field point as well as on the difference between the frequency of interest and the reference frequency. Accuracy criteria for a particular application are also presented. The computer time savings for our applications correspond to a factor of about 60 with accuracy being maintained.

Key words: Computations; focused; pressure field; transducer; ultrasound.

1. INTRODUCTION

Much of the research in our laboratory includes calculation of the acoustic pressure field resulting from pulsed focused or nonfocused transducers. For example, in a quantitative B-mode image texture simulation [1,2], determination of the pressure for a matrix of spatial positions and over a broad range of frequencies is required. These calculations involve numerical integration and can be very time consuming. A 2 cm x 2 cm image texture simulation for a 3.5 MHz single element focused transducer excited by a broadband pulse involves calculating the continuous wave pressure distributions for a matrix of about 5,000 spatial positions and 110 frequencies in the range from 1.5 MHz to 5.5 MHz. Using an experimentally-verified single integral expression for the acoustic pressure at a field point [3], calculation of the 550,000 complex pressure values requires about four hours on a VAX 785. A similar pressure calculation is employed in the method of data reduction for estimating acoustic backscatter coefficients used in our lab [4].

We previously developed and reported [5] a Taylor series expansion in frequency of an integral expression for the acoustic pressure at a point in the field of a nonfocused, disc-shaped transducer. In the present work, we present a more general Taylor series expansion of this expression for application to single element focused or nonfocused radiators with axial symmetry. A formula which allows easy determination of an unlimited number of terms is also presented.

0161-7346/87 $3.00

Time savings realized by applying the Taylor series depends on the specific application. For the texture simulation example above, pressure calculation time is reduced to about four minutes; a time savings factor of about sixty. Similar time savings result in determining backscatter coefficients. It should be noted that this time savings factor applies also to the work reported in reference [5] on nonfocused transducers. In the latter paper, a time savings factor of seven was estimated. Inefficiency in a computer program section, discovered after publication, led to this discrepancy.

A set of criteria are reported for a specific application that allow systematic determination of the off-axis distance to which acoustic pressure must be calculated and the number of Taylor series terms required to adequately represent the correct pressure calculation. These criteria can be used as a model for other applications.

It is important in computing pressure distributions in attenuating media to employ the attenuation coefficient at the frequency of interest. When accurate pulse shapes are required in attenuating media, accurately accounting for the frequency dispersion of phase speeds is also required [6]; this is true even though the percent shift in phase speed per MHz may be very small. In most laboratories, it is much easier to determine the frequency dependence of the attenuation coefficient of a material than to determine the frequency dependence of its phase speed. In the Taylor series expansion developed in this work, the Kramers-Kronig relations, as developed by Ginzberg [7], are employed to express the frequency-dependent phase speed in terms of the frequency-dependent attenuation coefficient.

2. THEORY

2.1 Representation of a Pulsed Pressure Beam

The derivation of the expression for acoustic pressure which is expanded in a Taylor series is presented in reference [3]. For the convenience of the reader, a summary of the relevant aspects is presented below.

Consider a pulsed single element piezoelectric transducer. When the (linear) Helmholtz equation applies, the acoustic pressure $p(\vec{r},t)$ for a field point at position $\vec{r}$ and time t, can be represented as the superposition of a set of continuous wave, sinusoidally-varying beams spanning some range of frequencies as follows:

$$p(\vec{r},t) = Re\left(\int_0^\infty B_0(\omega)A_0(\vec{r},\omega)e^{-i\omega t}d\omega\right). \tag{1}$$

Re means "Real part of," $B_0(\omega)$ is a complex superposition coefficient at frequency ω and $A_0(\vec{r},\omega)e^{-i\omega t}\ d\omega$ is a differential continuous wave solution of the Helmholtz equation for the particular transducer geometry involved.

Modeling the transducer as a set of equivalent monopole sources uniformly distributed across the face of the transducer and acting in unison results in $A_0(\vec{r},\omega)$ having the form

$$A_0(\vec{r},\omega) = \iint_S \frac{e^{ik|\vec{r}-\vec{r''}|}}{|\vec{r}-\vec{r''}|}\ dS'', \tag{2}$$

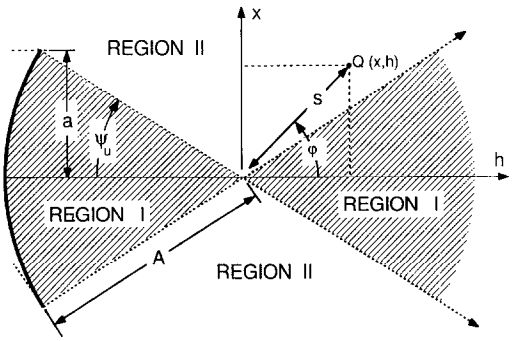

Fig. 1 Diagram showing the division of the focused transducer field into two regions, I and II. The axis of symmetry of the radiating element lies along the horizontal line. The origin of the (x, h) coordinate system lies on the axis of symmetry at the center of curvature. Also shown are various parameters involved in the single integral form of $A_0(\vec{r}, \omega)$ described in subsection 2.1.

where the integration is over the surface S of the transducer's active element and $\vec{r''}$ terminates on area element dS''. (Note: Both $\vec{r''}$ and $\vec{r}$ are position vectors extending from the origin of the coordinate system to the points specified.) $k = k_R + ik_I$ is the complex wavenumber in the propagating medium with real and imaginary parts $k_R = \omega/c(\omega)$ and $k_I = \alpha(\omega)$, respectively. The parameter $c(\omega)$ is the ultrasonic speed and $\alpha(\omega)$ is the amplitude attenuation coefficient at frequency ω.

If the radiating element has the form of a spherical cap with axial symmetry, the double integral in Eq. (2) can be reduced to the sum of a single integral and a nonintegral term having the form

$$A_0(\vec{r}, \omega) = \frac{2A}{s}\left(\int_{C'}^{D'} \gamma(r') e^{ikr'} dr' - \frac{i}{k} F\right) . \tag{3}$$

A is the radius of curvature of the radiating element and s is the distance from the radius of curvature to the field point Q at $\vec{r}$. (See figure 1 for a pictorial aid.) The quantities $C', D', \gamma(r')$, and F depend only on geometrical parameters and are independent of frequency and physical properties of the propagating medium. They are defined as follows:

$$C' \equiv \left[A^2 + s^2 + 2As\ \cos(\psi_u + \phi)\right]^{\frac{1}{2}},$$

$$D' \equiv \left[A^2 + s^2 + 2As\ \cos(\psi_u - \phi)\right]^{\frac{1}{2}},$$

$$\gamma(r') \equiv \cos^{-1}\left[\frac{h + (A^2 - a^2)^{\frac{1}{2}} - (r'^2 + s^2 - A^2)\frac{\cos\phi}{2s}}{\frac{\sin\phi}{2s}\left[4s^2r'^2 - (r'^2 + s^2 - A^2)^2\right]^{\frac{1}{2}}}\right], \quad and$$

$$F = \begin{cases} 0 \text{ for region I of figure 1} \\ \frac{\pi h}{|h|}\left(e^{ik\delta} - e^{ikd}\right) \text{ for region II of figure 1} \end{cases}$$

$$where\ \delta \equiv \left(A + \frac{hs}{|h|}\right) \quad and$$

$$d \equiv \left[A^2 + s^2 + 2As\cos(\psi_u - \frac{h}{|h|}\phi)\right]^{\frac{1}{2}} .$$

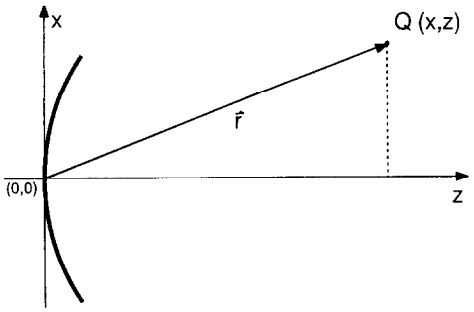

Fig. 2 Diagram showing the simplified coordinate system. The axis of symmetry of the radiating element lies along the horizontal line. Because of axial symmetry, a field point can be specified by its coordinates x and z where the origin is at the center of the radiating element.

The parameters ψ_u, ϕ, s, and h are shown in figure 1. Note that the h axis lies on the axis of symmetry of the radiating element and has its origin at the center of curvature of the radiating element.

For simplicity, it is convenient to define a new coordinate system, shown in figure 2, in which a new coordinate $z \equiv h - A$ replaces h. Note that x is not a Cartesian coordinate but is the distance from the z axis to Q and $r = \mid \vec{r} \mid = (x^2 + z^2)^{\frac{1}{2}}$.

In the limit as $A \rightarrow \infty$, $A/s \rightarrow 1$, $h/\mid h \mid \rightarrow -1$ and the radiating element becomes a nonfocusing disc. In this case,

$$C' \equiv \left[(a-x)^2 + z^2\right]^{\frac{1}{2}},$$

$$D' \equiv \left[(a+x)^2 + z^2\right]^{\frac{1}{2}},$$

$$\gamma(r') \equiv \cos^{-1}\left[\frac{-a^2 + r'^2 + x^2 - z^2}{2x(r'^2 - z^2)^{\frac{1}{2}}}\right],$$

$$\delta \equiv \left[(a-x)^2 + z^2\right]^{\frac{1}{2}} \quad and$$

$$d \equiv z\,.$$

2.2 Relationship Between Ultrasonic Phase Speeds and Attenuation Coefficients

Even though the fractional shifts are extremely small, the frequency dispersion of the ultrasonic speed in (attenuating) soft tissue is significant when accurate representations of ultrasonic pulse shapes are needed [6]. Ginzberg [7] has developed integral expressions, resulting from causality, relating the frequency-dependent ultrasonic speed to the frequency-dependent attenuation coefficient. Using our notation, Ginzberg's result is

$$\frac{1}{c(\omega)} - \frac{1}{c(\omega_0)} \cong \frac{2}{\pi} P \int_0^\infty \alpha(\omega') \left[\frac{1}{\omega'^2 - \omega^2} - \frac{1}{\omega'^2 - \omega_0^2}\right] d\omega' \qquad (4)$$

where P means "Principle value of", $c(\omega)$ is the speed of sound at frequency ω and $c(\omega_0)$ is the speed of sound at reference frequency ω_0. This is the form of the Kramers-Kronig relations employed in reference [6] yielding excellent agreement between theory and experiment.

A good first approximation for the frequency dependence of the attenuation coefficient, $\alpha(\omega)$, is a simple proportionality to frequency. A better approximation results from adding a quadratic term resulting in the form

$$\alpha(\omega) = \alpha_1\omega + \alpha_2\omega^2$$

where α_1 and α_2 are constants. Substituting this form of $\alpha(\omega)$ into Eq. (4) we have

$$\frac{1}{c(\omega)} = \frac{1}{c(\omega_0)} + \frac{2}{\pi}P\int_0^\infty \left[\frac{\alpha_1\omega' + \alpha_2\omega'^2}{\omega'^2 - \omega^2} - \frac{\alpha_1\omega' + \alpha_2\omega'^2}{\omega'^2 - \omega_0{}^2}\right] d\omega' \ .$$

The integrals can be evaluated and the result is

$$\frac{1}{c(\omega)} = \frac{1}{c(\omega_0)} + \frac{2\alpha_1}{\pi} \ ln\left(\frac{\omega_0}{\omega}\right) \ .$$

By expanding $\omega/c(\omega)$ in a Taylor series about ω_0 and keeping terms through the quadratic, the complex wavenumber can be expressed in the form

$$k(\omega, \alpha_1, \alpha_2) = \frac{\alpha_1\omega_0}{\pi} + \left(\frac{1}{c(\omega_0)} + i\alpha_1\right)\omega - \left(\frac{\alpha_1}{\pi\omega_0} - i\alpha_2\right)\omega^2 \ . \tag{5}$$

The reason for introducing the expansion of $\omega/c(\omega)$ is to simplify the Taylor series expansion of the acoustic pressure calculation as developed in the next section; i.e., higher order derivatives of k with respect to ω are zero.

2.3 The Taylor Series Expansion

The function which has been expanded in a Taylor series is

$$a_0(\vec{r}, \omega) \ \equiv \ e^{-ikr}A_0(\vec{r}, \omega)$$

where $A_0(\vec{r}, \omega)$ is in the form shown in Eq. (3) and $r \ = \mid \vec{r} \mid$. Following expansion, the result is then multiplied by e^{ikr} to recover $A_0(\vec{r}, \omega)$. The reason for expanding $a_0(\vec{r}, \omega)$ instead of $A_0(\vec{r}, \omega)$ is that the factor $e^{ikr'}$ in the integrand on the right of Eq. (3) generally contains a very large phase angle $k_R r' \ = \ \omega r'/c$. For example, at a typical frequency, say 3 MHz $= 6\pi \times 10^6$ radians/s, a typical ultrasonic speed of 1.5×10^5 cm/s and a typical value of $r' = 10$ cm, $k_R r' \ = \ 4\pi \ \times 10^2$ radians $\simeq$ 1,000 radians. In the computation of $e^{ik_R r'}$, a precision of seven significant digits in $k_R r'$ translates into only three or four significant digits in $e^{ik_R r'}$. When the factor e^{-ikr} is introduced, $e^{ik(r'-r)}$ is evaluated; $(r' - r)$ is typically on the order of 1 mm which means $e^{ik_R(r'-r)}$ would be on the order of 10 radians instead of 1,000 and two more significant digits are gained in the numerical evaluation of the exponential.

Shown below is the general form of the Taylor series expansion in frequency, ω, the reference frequency being ω_0.

$$a_0 \ = \ a_0(\vec{r}, \omega) \ \equiv \ e^{-ikr}A_0(\vec{r}, \omega) \ =$$

$$a_0(\vec{r},\omega_0) \; + \; \left.\frac{\partial a_0}{\partial \omega}\right|_{\omega=\omega_0} (\omega-\omega_0) \; + \; \frac{1}{2}\left.\frac{\partial^2 a_0}{\partial \omega^2}\right|_{\omega=\omega_0} (\omega-\omega_0)^2$$

$$+ \; \frac{1}{3!}\left.\frac{\partial^3 a_0}{\partial \omega^3}\right|_{\omega=\omega_0} (\omega-\omega_0)^3 \; + \; \cdots$$

Since all the frequency and propagating medium dependencies of $a_0(\vec{r},\omega)$ are contained in the complex wavenumber, k, all the needed partial derivatives of $a_0(\vec{r},\omega)$ can be found using the chain rule. For example,

$$\frac{\partial a_0}{\partial \omega} = \frac{\partial k}{\partial \omega}\,\frac{da_0}{dk}$$

$$\frac{\partial^2 a_0}{\partial \omega^2} = \frac{\partial}{\partial \omega}\left(\frac{\partial a_0}{\partial \omega}\right) = \frac{\partial^2 k}{\partial \omega^2}\,\left(\frac{da_0}{dk}\right)^2 + \left(\frac{\partial k}{\partial \omega}\right)^2\,\frac{d^2 a_0}{dk^2}\;.$$

As a result of expressing k as a quadratic function of ω (see Eq. 5), considerable simplification results because

$$\frac{\partial^n k}{\partial \omega^n} = 0 \quad for \; n > 2\;.$$

For the integral portion of a_0 the only k dependence is in the exponential portion of the argument. Thus, the n^{th} derivative of the integral part of a_0 is

$$\frac{d^n}{dk^n}\left(\int_{C'}^{D'} \gamma(r'-r)e^{ik(r'-r)}dr'\right) = i^n \int_{C'}^{D'} (r'-r)^n\;\gamma(r'-r)e^{ik(r'-r)}dr'\;.$$

The n^{th} derivative of the nonintegral term in a_0 has the form

$$\frac{d^n}{dk^n}\left(\frac{i}{k}F\right) = i(-1)^n\; n!\; k^{-n-1}\;\sum_{m=0}^{n}\frac{(-i)^m}{m!}\left(\delta^m e^{ik\delta} - d^m e^{ikd}\right)k^m\;.$$

Thus, the n^{th} derivative of $a_0(\vec{r},\omega)$ with respect to k is

$$\frac{d^n}{dk^n}(a_0) = i^n \int_{C'}^{D'} (r'-r)^n\;\gamma(r'-r)e^{ik(r'-r)}dr'$$

$$+i(-1)^n\; n!\; k^{-n-1}\;\sum_{m=0}^{n}\frac{(-i)^m}{m!}\left(\delta^m e^{ik\delta} - d^m e^{ikd}\right)k^m\;.$$

3. ACCURACY CONSIDERATIONS

Use of a Taylor series to represent a function requires an understanding of acceptable error limits for the particular application. For an application involving accurate determination of backscatter coefficients from echo signal data [4] a well-defined set of criteria has been developed and is presented as an example.

One of the principle relations involved in the method of data reduction for estimating acoustic backscatter coefficients is given in Eq. (17) of reference [4]. The denominator of this equation contains an integral over volume of the form

$$\iiint [A_0(\vec{r},\omega)]^2 \, d^3\vec{r}$$

where $A_0(\vec{r},\omega)$ is given by Eq. (2) above and it is the accuracy with which this integral is determined that is of concern. The integral includes the entire volume over which scatterers may exist. The volume that contributes significantly to this integral is limited axially by the use of a time gate applied to the echo signal as well as by the decrease in $|| A_0(\vec{r},\omega) ||$ with increasing distance, x, from the beam axis. Employing the coordinate system of figure 2, $\vec{r} = \vec{r}(x,\theta,z)$ where x, θ and z are cylindrical coordinates. Since the beam is axially symmetric, integration with respect to θ yields a factor of 2π. Thus,

$$\iiint [A_0(\vec{r},\omega)]^2 \, d^3\vec{r} = 2\pi \iint [A_0(x,z,\omega)]^2 \; x \; dx \; dz \; . \tag{6}$$

Two accuracy criteria are presented below followed by a procedure for determining values of a pair of parameters for which the criteria are fulfilled. These criteria assure that the value of the integral in Eq. (6) will be represented with sufficient accuracy when the Taylor series approximation for $A_0(x,z,\omega)$ is employed. The pair of parameters are

1. a minimum coordinate, $x = x_m$, through which the x integration in Eq. (6) must be carried out and
2. the corresponding minimum number of terms, N, in the Taylor series.

First, some preliminary studies were done in which various axially symmetric ultrasonic sources were considered, both experimentally and theoretically. Two general observations were made. First, for sufficiently large x, the envelope of $|| A_0(x,z,\omega) || \rightarrow 0$ as x increases. Second, for each axial distance z and frequency ω there is a characteristic spacing of off-axis minima, or side lobe widths, $\Delta x(z,\omega)$. It was also found that, for a given geometry of the radiating element, the dependence of Δx on z and ω can be established quite well by finding Δx for a grid with spacings of about 1 MHz and 2 cm in ω and z, respectively. The above observations have played a key role in the development of the accuracy criteria and in the procedure for establishing required values of x_m and N.

The two criteria are applied throughout the ranges of interest of z and ω. These criteria are

$$J_n(N) \equiv \frac{| I_n(N+1) - I_n(N) |}{I_n(N+1)} \leq 0.2 \;\; and$$

$$K_n(N) \equiv \frac{I_n(N)}{\sum_{j=1}^{n} I_j(N)} \leq 0.03$$

$$\text{where } I_j(N) \equiv \int_{(j-1)\Delta x}^{j\Delta x} || A_{0,N}(x,z,\omega) ||^2 \; x \; dx$$

and $A_{0,N}(x,z,\omega)$ is the approximation to $A_0(x,z,\omega)$ keeping N terms in the Taylor series. (Notice that since $x \geq 0$, we have $j \geq 1$.)

The procedure for applying the criteria contains six ordered steps, and is applied beginning with the lowest value of n ($n \geq 2$) such that the points having coordinates $x = (n-1)\Delta x$ and z lies in region II of figure 1. ($n = 1$ is not included because K_n would always equal 1.) The six steps are as follows:

1. Select a number of terms, N, to be included in the truncated Taylor series; N can be as low as 1.
2. Set $n = 2$.
3. If $J_n \leq 0.2$, go to step 5 below.
4. If $J_n < 0.2$, increment N by 1 and go to step 2.
5. If $K_n \leq 0.03$, then the values for n and N are satisfactory, and this is the last step needed.
6. If $K_n > 0.03$, increment n by 1 and go to step 3.

If and when values of n and N are found resulting in satisfying the two criteria, then this N is the number of Taylor series terms to be kept and $x_m = n\Delta x$.

4. RESULTS

Because of the large number of variables involved, selection of an optimal set of examples to efficiently illustrate the value of the Taylor series representation is a difficult task. Focused transducers with approximately 11 cm radius of curvature and 19 mm projected diameter are used in our laboratory for measuring backscatter coefficients and generating B-mode texture images. For the results presented here, the transducer modeled has these values of the radius of curvature and projected diameter. The reference frequency for the Taylor series is $\omega_0 = 5.0$ MHz, and the propagating medium is assumed to exhibit an ultrasonic speed of 1540.0 m/s at 5.0 MHz and attenuation coefficient constants $\alpha_1 = 0.5$ dB/cm/MHz and $\alpha_2 = 0$ where $\alpha(\omega) = \alpha_1\omega + \alpha_2\omega^2$.

Before proceeding, it should be noted that only 16 Taylor series terms have been programmed to date primarily because 16 terms are sufficient for our current applications.

Figures 3–11 show comparisons between Taylor series approximations to $A_0(\vec{r},\omega) = A_0(x,z,\omega)$ (dashed lines) and the correct values for $A_0(\vec{r},\omega)$ (solid lines), the latter obtained with the integration in Eq. (3) performed numerically using Gaussian quadrature. In each figure, part (a) shows the modulus of $A_0(\vec{r},\omega)$ and part (b) its phase (in cycles). Each figure corresponds to specific values of the axial distance, frequency, and the number of terms kept in the series, and $A_0(\vec{r},\omega)$ is shown as a function of off-axis distance; such plots are known as lateral beam profiles.

An important didactic aspect of figures 3–7 is that successive figures involve a change in only one of the three parameters; z, $\omega - \omega_0$ and N. It is hoped that this will convey

Table I. Values of the axial distance from the transducer, z, the frequency difference, $\omega-\omega_0$, the frequency of evaluation, ω, and the number of terms in the series, N, corresponding to figures 3–7. The reference frequency was ω_0=5.0 MHz in all cases.

Fig. No.	z (cm)	$\omega-\omega_0$ (MHz)	ω (MHz)	N
3	4.0	-0.6	4.4	8
4	4.0	-0.6	4.4	16
5	4.0	-1.0	4.0	16
6	12.0	-1.0	4.0	16
7	12.0	-2.0	3.0	16

insight into the relation between the three parameters and the accuracy of the Taylor series approximation. Table I summarizes the values of z, $\omega-\omega_0$, and N for each of these figures. Notice that all values of $\omega-\omega_0$ are negative. This is because, for a given number of terms kept in the series, sufficient accuracy at $\omega-\omega_0 = -|\omega-\omega_0|$ generally assures accuracy at $\omega-\omega_0 = |\omega-\omega_0|$.

Figure 3 shows plots of the modulus and phase of $A_0(\vec{r},\omega)$ for an axial distance of z=4.0 cm comparing the correct solution for $A_0(\vec{r},\omega)$ at 4.4 MHz and the 8 term

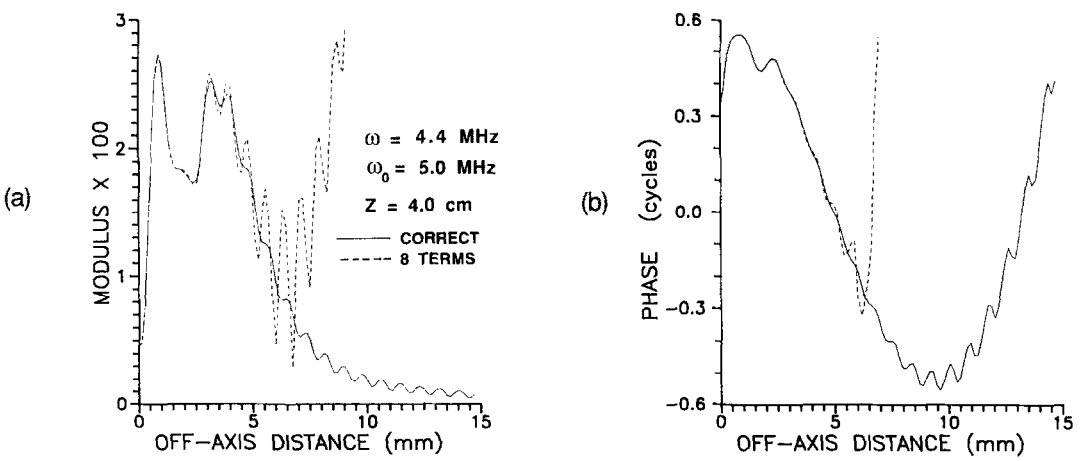

Fig. 3 Graphs of the modulus (a) and phase (b) of $A_0(\vec{r},\omega)$ comparing the correct calculation (solid line), obtained by direct numerical integration, with an 8 term Taylor series calculation (dashed line). The frequency at which the computations were made was 4.4 MHz, and the Taylor series reference frequency was 5.0 MHz. The axial distance was z=4.0 cm. The propagating medium was taken to be tissue–like with an ultrasonic speed of 1540 m/s at 5.0 MHz and an attenuation coefficient slope of 0.5 dB/cm/MHz.

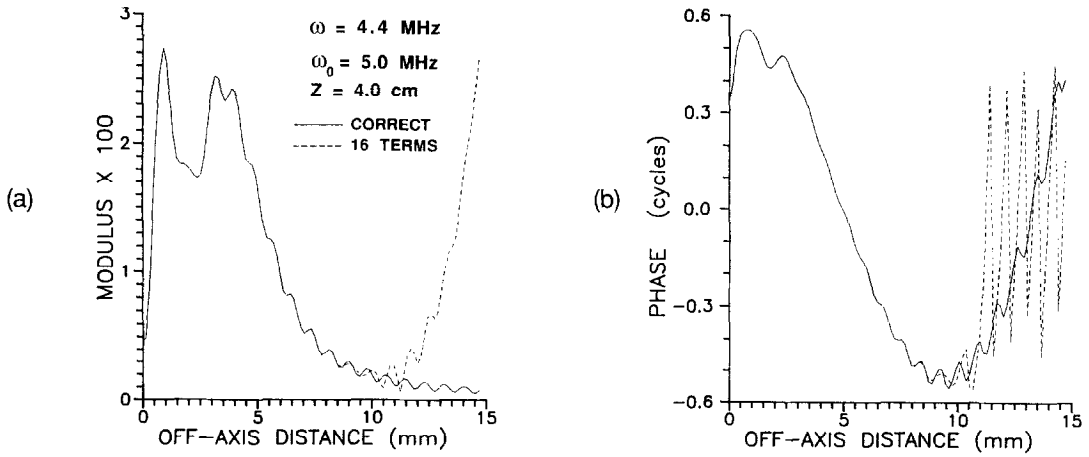

Fig. 4 Graphs comparing a 16 term Taylor series (dashed line) with the correct result (solid line). All other parameters the same as figure 3.

Taylor series representation for 4.4 MHz. In figure 3a the Taylor series representation is shown only through about 9 mm off axis and in figure 3b through about 6.5 mm, due to divergence of the truncated Taylor series with increasing x. For this set of parameters, eight Taylor series terms would not be sufficient for most applications.

Figure 4 shows plots for a comparison under conditions identical to those in figure 3 (axial distance of 4.0 cm, frequency of 4.4 MHz) except 16 Taylor series terms are kept. Sixteen terms appear to be adequate for this set of parameters as long as the modulus is taken to be zero beyond, say, 10 mm.

In figure 5, all parameters are the same as those in figure 4 except that ω=4.0 MHz instead of 4.4 MHz. The considerable loss of accuracy due to the larger value of $|\omega-\omega_0|$ is demonstrated.

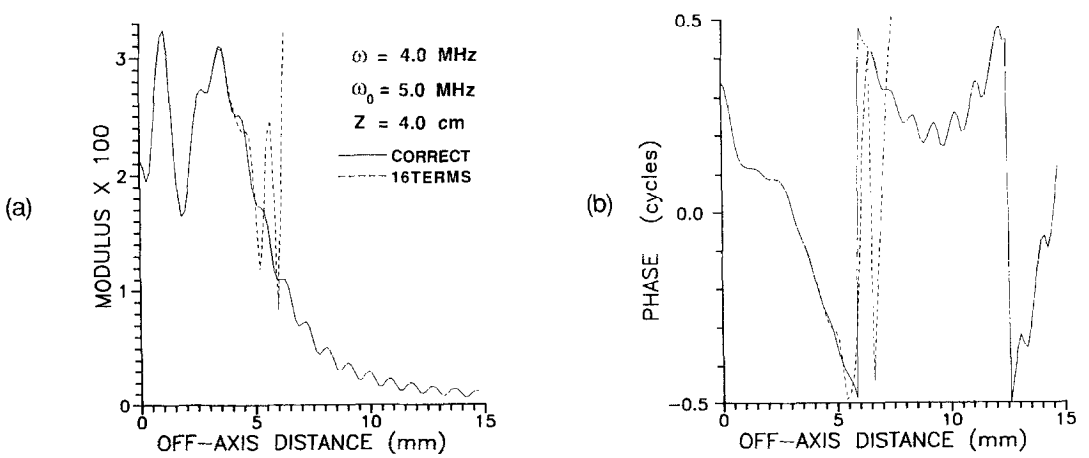

Fig. 5 Graphs comparing a 16 term Taylor series (dashed line) with the correct result (solid line) for a frequency of 4.0 MHz. All other parameters the same as figure 3.

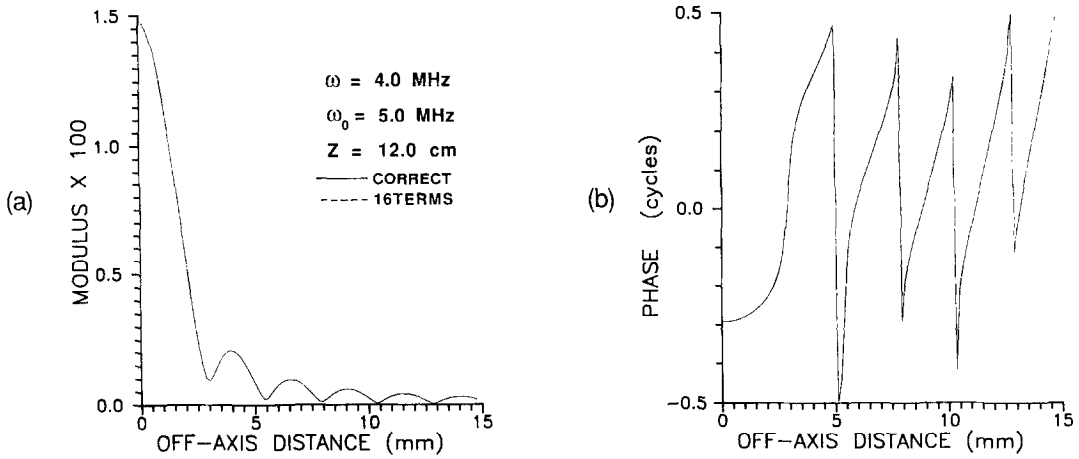

Fig. 6 Graphs comparing a 16 term Taylor series (dashed line) with the correct result (solid line) for an axial distance of 12.0 cm. All other parameters the same as figure 5.

In figure 6, all parameters are the same as those in figure 5 except the axial distance is now 12.0 cm which is in the focal region of the transducer modeled. For this set of parameters no distinction is seen between the Taylor series result and the correct values. For this combination of parameters, keeping 16 terms seems to constitute an "overkill."

The plots in figure 7 are for the same axial position and number of terms as in figure 6 except $\omega = 3.0$ MHz making $\omega - \omega_0$ now -2.0 MHz. Reasonably good accuracy is maintained by the 16 term Taylor series out to an off-axis distance of 10 or 11 mm for this case in which the value of $| \omega - \omega_0 |$ is rather large. This accuracy is apparently related to the fact that z=12 cm is in the focal region of the transducer.

In figures 8–11 are shown plots which illustrate the effectiveness of applying the procedure for assuring accuracy of the Taylor series for the specific situation described

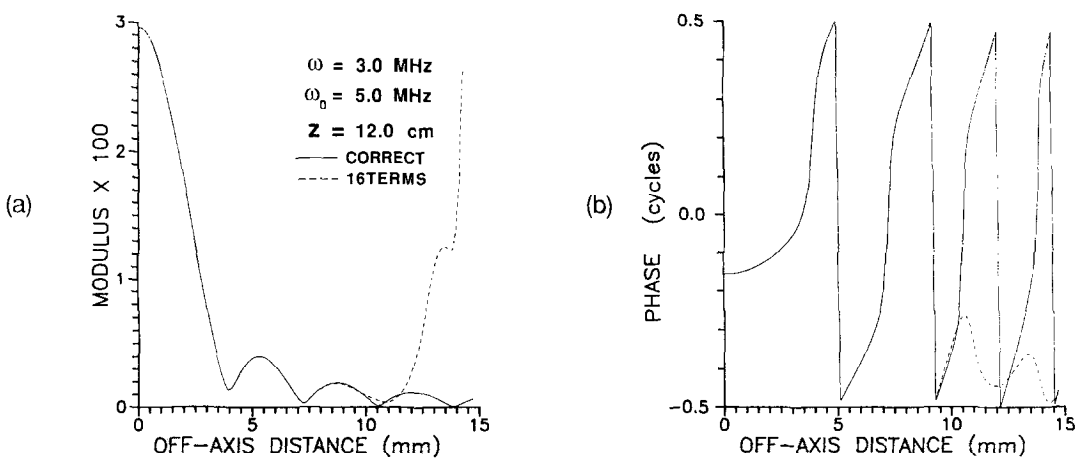

Fig. 7 Graphs comparing a 16 term Taylor series (dashed line) with the correct result (solid line) for a frequency of 3.0 MHz. All other parameters the same as figure 6.

Table II. Values of the axial distance from the transducer, z, the frequency difference, $\omega-\omega_0$, the frequency of evaluation, ω, and the number of Taylor series terms, N, required to meet the accuracy criteria corresponding to figures 8–11. The reference frequency was ω_0=5.0 MHz. The accuracy criteria, however, were not met with fifteen terms for the conditions shown in figures 11.

Fig. No.	z (cm)	$\omega-\omega_0$ (MHz)	ω (MHz)	N
8	6.0	-0.5	4.5	5
9	6.0	-1.0	4.0	15
10	12.0	-1.0	4.0	8
11	12.0	-2.0	3.0	—

in section 3. Each figure shows plots of the modulus and phase of $x\ A_0^2(\vec{r},\omega)$. The solid lines correspond to correct values and the dashed line to the Taylor series.

To provide insight into the relation between z, $\omega-\omega_0$, and N, only z or $\omega-\omega_0$ was changed from one figure to the next for figures 8–11. Table II summarizes the values of z,$\omega-\omega_0$ and the number of terms, N, required to meet the criteria.

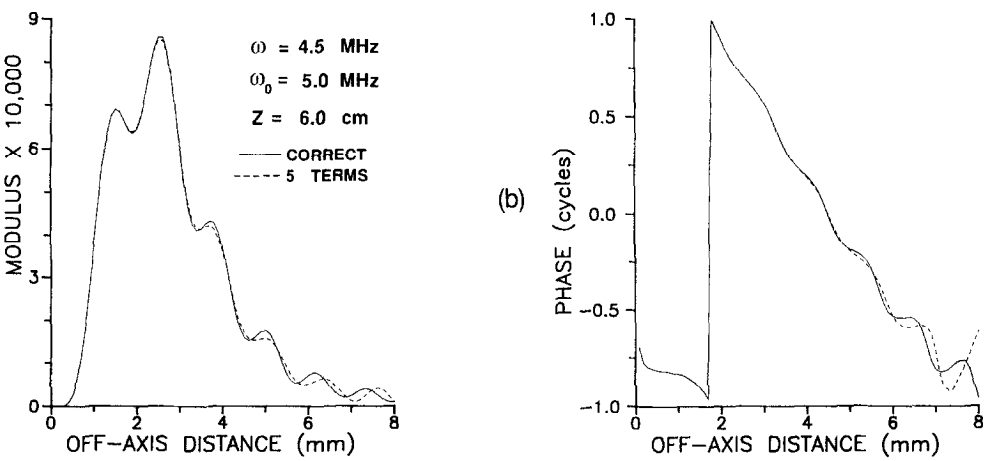

Fig. 8 Graphs illustrating the effectiveness of the procedure described in section 3 for assuring the accuracy of the Taylor series approximation for $A_0(\vec{r},\omega)$. In (a) the modulus of $[x\ A_0^2(\vec{r},\omega)]$ is plotted as a function of off-axis distance x, and in (b) the phase of $[x\ A_0^2(\vec{r},\omega)]$ is plotted. The correct solutions are shown as solid lines and the Taylor series result as dashed lines. The number of terms kept in the Taylor series was 5 which was the minimum number required to satisfy the accuracy criteria. Calculations were made for an axial distance of 6.0 cm in a tissue-like medium. ω=4.5 MHz, and the Taylor series reference frequency ω_0 was 5.0 MHz. The criteria were met with $J_5(5)$=0.10 and $K_5(5)$=0.019 which occurred 8 mm off axis.

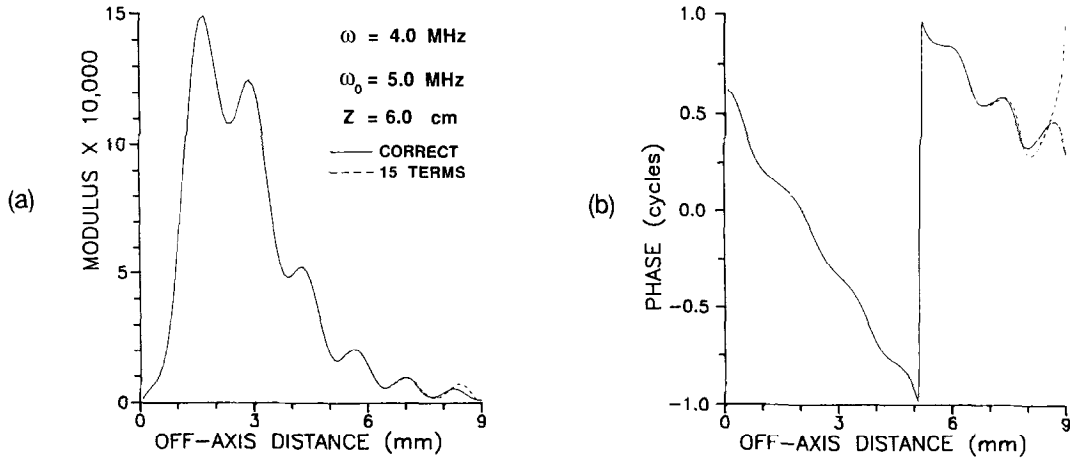

Fig. 9 Graphs illustrating the effectiveness of applying the Taylor series accuracy criteria for ω=4.0 MHz, all other parameters being the same as for figure 8. The accuracy criteria were met when $J_5(15)$=0.14 and $K_5(15)$=0.016 which occurred 9 mm off axis when 15 terms were used.

In figure 8, the axial distance is 6.0 cm and ω= 4.5 MHz. Five Taylor series terms were required to meet the accuracy criteria resulting in $J_5 = 0.10$ and $K_5 = 0.019$.

Figure 9 shows a comparison for the same axial distance but for ω= 4.0 MHz instead of 4.5 MHz. Fifteen Taylor series terms were required resulting in $J_5 = 0.14$ and $K_5 = 0.016$.

Figure 10 illustrates the reduced number of terms required to represent a 4.0 MHz beam profile in the focal region; in this case z=12.0 cm. The accuracy criteria were met with only 8 terms in the series and $J_4 = 0.17$ and $K_4 = 0.018$.

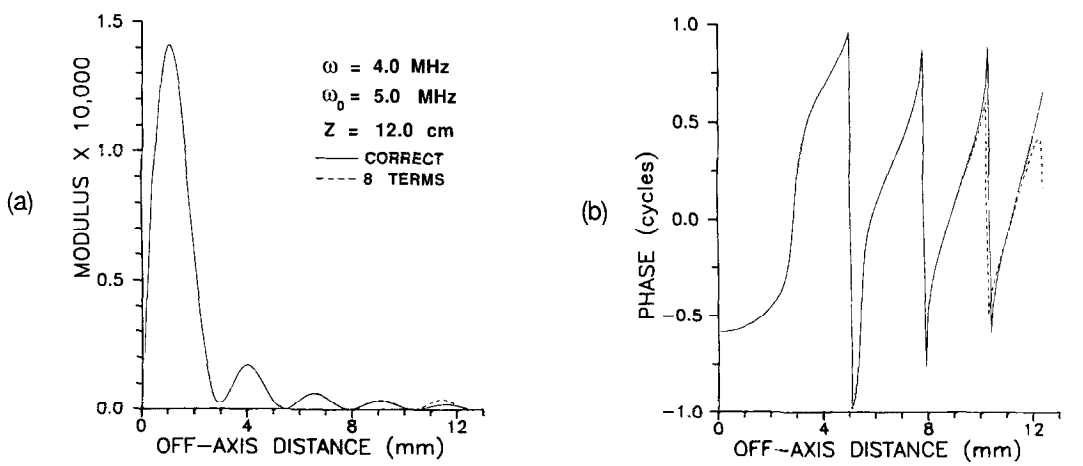

Fig. 10 Graphs illustrating the effectiveness of applying the Taylor series accuracy criteria at an axial distance z=12.0 cm, all other parameters being identical to those of figure 9. The accuracy criteria were met when $J_4(8)$=0.17 and $K_4(8)$=0.018 which occurred 15 mm off axis when 8 terms were used.

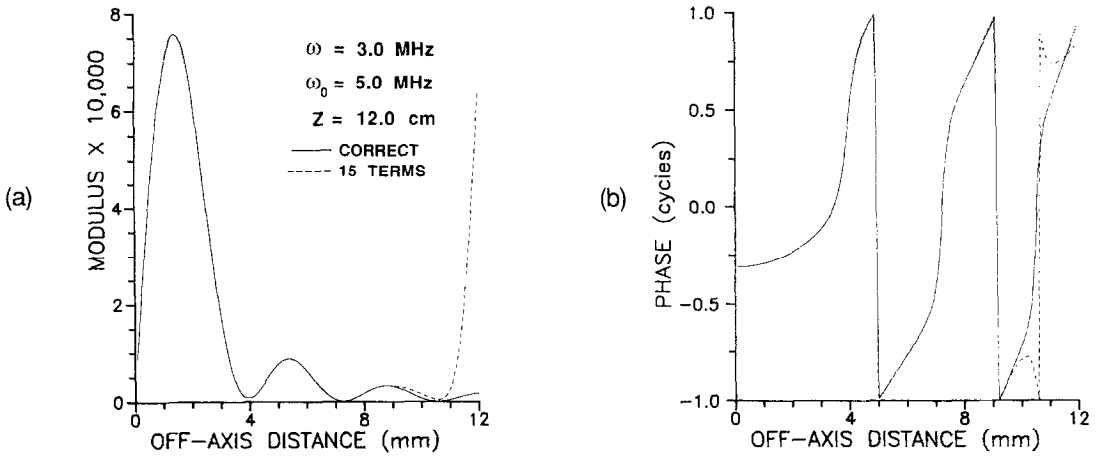

Fig. 11 Graphs illustrating the effectiveness of applying the Taylor series accuracy criteria for ω=3.0 MHz; all other parameters are the same as those employed in figure 10. The accuracy criteria were not met in the third subinterval when 15 terms were kept. For that subinterval $J_3(15)$=3.38 and $K_3(15)$=0.043. In the second subinterval, however, $J_2(15) = 8 \times 10^{-4}$ and a less stringent criterion for $K_n(N)$ could have been met.

Figure 11 shows the result of applying these criteria again at z=12.0 cm, but ω=3.0 MHz instead of 4.0 MHz. The accuracy criteria were not met in the last subinterval: for Δx extending from 8 to 12 mm, J_3 = 3.38 and K_3 = 0.043 for a fifteen term series. Excellent agreement was found though about 10 mm off axis, however.

In figure 12 are shown zones of accuracy for fixed values of N resulting from applying the accuracy criteria. The reference frequency was 5.0 MHz. Frequency is plotted versus

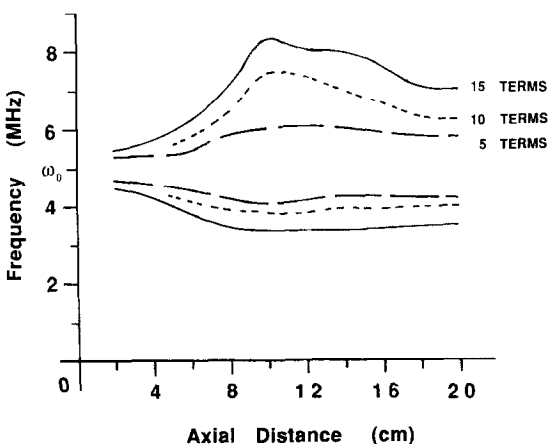

Fig. 12 Plot illustrating the ranges of frequencies for which the accuracy criteria of section 3 were met for 5, 10 and 15 term Taylor series as a function of axial distance from the transducer in a tissue-like medium. For example, the accuracy criteria are satisfied for N=10 and z=10 cm from ω=3.8 MHz through 7.5 MHz. The Taylor series reference frequency was 5.0 MHz. These results depend on the transducer geometry.

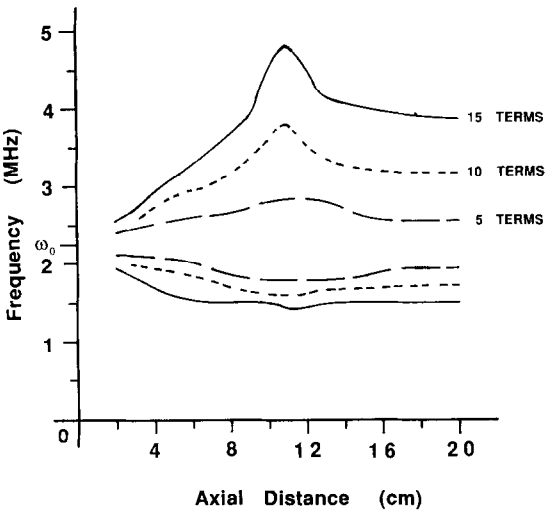

Fig. 13 Plot illustrating the ranges of frequencies for which the accuracy criteria of section 3 were met for 5, 10 and 15 term Taylor series as a function of axial distance from the transducer in a tissue-like medium. For example, the accuracy criteria are satisfied for N=10 and z=10 cm from ω=1.6 MHz through 3.7 MHz. The Taylor series reference frequency was 2.25 MHz. These results depend on the transducer geometry.

axial distance, z, for N=5 (long dash lines), N=10 (short dash lines), and N=15 (solid lines). Thus, for example, the accuracy criteria are satisfied for N=10 and z=10 cm from ω=3.8 MHz through 7.5 MHz.

In figure 13 is shown the same type of plot as shown in figure 12 except that in this case the reference frequency was 2.25 MHz.

5. DISCUSSION

Each of the figures 3–7 has illustrated that the truncated Taylor series is in very good agreement on axis and for some range of distances off axis. However, beyond some off axis distance, large discrepancies can develop; this off-axis distance depends on $\omega - \omega_0$, the axial distance, and the number of terms kept in the series.

Figures 3, 4, and 5 illustrate the effectiveness of the Taylor series representation in the near field. The axial distance, z, is 4.0 cm. The correct modulus of the pressure varies greatly out to almost an off-axis distance, x, of 5 mm, and beyond x=10 mm the modulus is very small and decreases with increasing x. Adequate accuracy through x=10 mm was obtained only when the maximum number of terms available in this study (16) were kept in the series, and this was true only for a modest difference between ω and ω_0 ($\omega - \omega_0$= -0.6 MHz). For $\omega - \omega_0$= -1.0 MHz, agreement of series and correct values exists only out to x=4 or 5 mm.

Figures 6 and 7 are beam profiles at z=12 cm which is in the focal region of the transducer. The results illustrate that the Taylor series approximation is more effective than in the near field for a fixed number of terms kept. In each case, the full 16 terms

were used and $\omega - \omega_0$ was varied. For $\omega - \omega_0 = -1.0$ MHz in figure 6, no significant difference exists between the correct and truncated series results out to x=15 mm. For $\omega - \omega_0 = -2.0$ MHz, the Taylor series approximation diverges abruptly beyond 11 mm. However, if accuracy through the second side lobe is adequate for the application involved, then the Taylor series solution corresponding to figure 7 could be used out to, say, x=11 mm and the pressure modulus set equal to zero for $x > 11$ mm.

In computing acoustic pressure distributions for application in estimating backscatter coefficients it is necessary to know how far off axis to calculate pressure profiles so that a sufficient number of terms are included to avoid the divergence illustrated in figures 3, 4, 5 and 7. Figures 8–10 show that when the accuracy criteria of section 3 are employed, excellent agreement is found at all off-axis points within x_m. Figure 11 illustrates that when these criteria are not met, excellent agreement may still exist through some acceptable off-axis distance and increasing the maximum allowable values of $J_n(N)$ and $K_n(N)$ might be justified.

Figures 12 and 13 show the dependence on axial distance of the zone of frequencies within which the Taylor series with N=5, 10, or 15 terms satisfies the accuracy criteria of section 3. Two general features are worth noting. First, for any N, the extent of the zone rapidly decreases as z decreases in the near field. Second, the zone is not symmetric about ω_0 in the focal region and beyond, particularly for the higher values of N; this asymmetry is especially significant for the case of ω_0=2.25 MHz in figure 13. Because of the asymmetry of the frequency zones in figures 12 and 13, the choice of ω_0 will depend on the frequency range over which accuracy is desired and this reference frequency will not in general be in the center of the range.

6. CONCLUSIONS

The Taylor series expansion in frequency of the single integral pressure beam solution for focused transducers provides a means of greatly increasing computer time savings. However, establishment of accuracy criteria corresponding to the particular application involved should be done before introducing the Taylor series representation into a computer program. Such criteria are crucial because of the considerable number of parameters which influence the accuracy (e.g., axial and off-axis distances, and $\Delta\omega$).

ACKNOWLEDGEMENTS

We gratefully acknowledge the assistance of Colleen Schutz for her help in typing the manuscript. This work was supported in part by grants RO1–CA39224 and RO1–CA25634.

REFERENCES

[1] Goodsitt, M.M., Madsen, E.L. and Zagzebski, J.A., A three dimensional model for generating the texture in B–scan ultrasound images, *Ultrasonic Imaging* **5**, 253–279 (1983).

[2] Zagzebski, J.A., Madsen, E.L. and Goodsitt, M.M., Quantitative tests of a three dimensional gray scale texture model, *Ultrasonic Imaging* **7**, 252–263 (1985)

[3] Madsen, E.L., Goodsitt, M.M. and Zagzebski, J.A., Continuous waves generated by focused radiators, *J. Acoust. Soc. Am.* **70**, 1508–1517 (1981).

[4] Madsen, E.L., Insana, M.F. and Zagzebski, J.A., Method of data reduction for accurate determination of acoustic backscatter coefficients, *J. Acoust. Soc. Am.* **76**, 913–923 (1984).

[5] Madsen, E.L., Hall, T.J., Zagzebski, J.A. and Insana, M.F., Use of taylor series expansions for time savings in computation of accurate transducer pressure fields, *IEEE Trans. Ultrasonics, Ferroelectrics Frequency Control UFFC* **34**, 301–308 (1987).

[6] Goodsitt, M.M., Madsen, E.L. and Zagzebski, J.A., Field patterns of pulsed focused ultrasonic radiators in attenuating and nonattenuating media, *J. Acoust. Soc. Am.* **71**, 318–329 (1982).

[7] Ginzberg, V.L., Concerning the general relationship between absorption and dispersion of sound waves, *Soviet Phys. Acoustics* **1**, 32–41 (1955).